Unconventional superfluid phases and the phase dynamics in spin-orbit-coupled Bose systems

Anirban Dutta[1] and Saptarshi Mandal[1,2]

[1]*Department of Theoretical Physics, Indian Association for the Cultivation of Science, Jadavpur, Kolkata 700032, India*

[2]*The Abdus Salam International Center for Theoretical Physics, P.O Box 586, I-34151 Trieste, Italy*

(Received 15 April 2013; published 10 December 2013)

We study the phase and amplitude distribution of superfluid (SF) order parameters for spin-orbit-coupled two species bosons in a two-dimensional finite-size square lattice using inhomogeneous mean-field analysis. We demonstrate how phase distribution of the SF order parameter evolves as we tune the spin-orbit coupling γ and t, the spin-independent hopping in the strong-coupling limit. For $t \gg \gamma$, we find the homogeneous superfluid phase where the phase of the SF order parameter is uniform. As we increase γ, spatial inhomogeneity in the phases of the SF order parameter grows leading to a twisted superfluid phase. For $t \sim \gamma$, competing orderings in the phase distribution are observed. At large γ limit, a ferromagnetic stripe ordering appears along the diagonal. We explain that this is due to the frustration bought in by the spin-orbit interaction. Isolated vortex formation is also shown to appear. The effect of the detuning field δ on the distribution of phases and amplitudes of the order parameter has also been studied. We also investigate the possible collective modes for this finite-size system. In a deep superfluid regime we derive the Euler-Lagrange equation of motion for the phases and the dynamics of lowest normal modes are discussed.

DOI: 10.1103/PhysRevA.88.063619 PACS number(s): 03.75.Lm, 05.30.Jp, 05.30.Rt

I. INTRODUCTION

The recent advancement in optical lattice experiments to investigate the idealized strongly correlated many-body system has initiated a great interest among the condensed-matter community [1]. Starting from mimicking a simple tight-binding Hamiltonian in a periodic lattice, it can now create more complex situations seen in real materials. Creation of artificial Abelian or non-Abelian gauge fields and density-density interaction are some of them to mention [2,3]. Experimental realization of Mott-insulator to superfluid transition for ultracold bosons [4,5] in such a system became a paradigm of itself. Recently, there has been experimental realization to simulate tunable spin-orbit coupling in neutral bosons in an optical lattice [6,7]. This is remarkable because it is known that for real material spin-orbit coupling is essentially an intrinsic [8] property of the material and could not be controlled. The spin-orbit interaction can change the physical properties of the system dramatically. In an optical lattice, the spin-orbit coupling is achieved by Raman laser induced transitions between the two internal states of a neutral bosonic atom. The resulting spin-orbit interaction could be purely Rashba [9] type or Dresselhaus [10] type or a suitable combination of both.

The physical implications of such spin-orbit interaction have been studied extensively recently [11–16] in various contexts. In the Mott regime it is shown to support exotic magnetic textures, such as vortex crystals and Skyrmion lattice [11–13]. The signature of the Mott-insulator to superfluid transition has been shown to be associated with precursor peaks in momentum distributions [17–20]. Various other equilibrium and nonequilibrium dynamics have also been analyzed which could have interesting experimental signatures [21]. Boson fractionalization has also been proposed and formation of twisted superfluid phases has been noticed as a result of spin-orbit interaction [20,22]. It may be mentioned that for the fermionic case interesting many-body dynamics have also been observed [23] in the presence the spin-orbit interaction.

The Mott-insulator to superfluid transition is well captured by the Bose-Hubbard model [24–26]. There is already a large amount of work done which investigated the low-energy properties of such a Bose-Hubbard model [27–30]. However, much of these works were mainly aimed at looking into the systems which are thermodynamically large and are in weak-coupling regime. In this work, we look into the effect of spin-orbit interaction of two-component bosons in a strong-coupling limit for finite-size systems. We are motivated to look into microscopic manifestation of the spin-orbit interaction and various ramifications of the superfluid order parameter for a finite-size system in different parameter regimes. For this we employ Gutzwiller projected inhomogeneous mean-field treatment [27,31], which seems to be pertinent for such a small system size. We work in the strong-coupling limit where the Hubbard interaction is the highest energy scale of the problem. This limit enables us to take the number of states in the Gutzwiller projected state to be necessary minimal. The Hamiltonian, H, we work with can be written as the sum of two terms, H_0 and H_1, which are given below [7,20]:

$$\begin{aligned} H_0 &= \sum_{ia} -\mu n_{ia} + U n_{ia}(n_{ia}-1) + \lambda U \sum_i n_{i1} n_{i2} \\ &\quad - \sum_{\langle ij\rangle_a} t_a b_{ia}^\dagger b_{ja}, \\ H_1 &= i\gamma \sum_{\langle ij\rangle} \Psi_i^\dagger \hat{z} \cdot (\vec{\sigma} \times \vec{d}_{ij}) \Psi_j \\ &\quad + \sum_i (\delta \Psi_i^\dagger \sigma_y \Psi_i - \Omega \Psi_i^\dagger \sigma_z \Psi_i). \end{aligned} \tag{1}$$

Here $\Psi_i = (b_{i1}, b_{i2})$ with $b_{i\alpha}$ representing the bosonic annihilation operator for the species α (with α taking values 1 and 2). As usual $n_{i\alpha}$ denotes the number operator for respective bosons. In H_0, μ represents the chemical potential, Ω is the Zeeman shift between the two species, U is the intraspecies interaction, and λ is the on-site interspecies interaction. The

last term in H_0 represents the usual spin conserved hopping interaction. The terms in H_1 describe three different types of spin-orbit interaction. The first term with coupling strength γ describes the usual Rashba [9] spin-orbit interaction. $\vec{d}_{ij}$ denotes the vector pointing from site i to site j. The dot product with the unit vector $\hat{z}$ signifies that the system lies in the x-y plane. The spin-dependent hopping process for this system could be written as $\Psi_i^\dagger R_{ij}\Psi_j$. The matrix R_{ij} describes the hopping process in background non-Abelian gauge field. Here $R_{ij} = e^{\vec{A}\cdot(\vec{r}_i-\vec{r}_j)}$ with $\vec{A} = \alpha(\sigma_y,-\sigma_x,0)$ [11,12]. The diagonal terms coming from R_{ij} contribute to the spin conserved hopping process and the off-diagonal terms constitute the spin-dependent hopping process with $\gamma \sim \sin\alpha$. The last two terms in the expression of H_1 describe the effect of transverse Zeeman field in y-z plane with strength δ and Ω in the y and z directions, respectively. The presence of these two terms makes the Hamiltonian different than what has been studied recently [11,12]. Presence of Ω breaks the degeneracy between two species of bosons and results in a unique nondegenerate Mott state. It may also be noted that, while Refs. [11,12] studied the properties of the effective spin Hamiltonian deep inside the Mott phase in the strong-coupling limit, our aim is to look into a superfluid regime taking into account the effect of Ω and δ. While taking into the effect of δ and Ω in our model, we have in our mind the experimental realization of Ref. [7] where two species of bosons refers to $m_F = 0$ and $m_F = -1$ hyperfine states of $F = 1$ Rb atoms. The spin-orbit coupling is achieved by applying two Raman lasers whose frequencies are detuned by δ compared to the Raman transition frequency of $m_F = 0$ and $m_F = -1$ hyperfine states of Rb atoms. In addition to the usual spin-dependent hopping process, these lasers also create an effective Zeeman field in the y-z plane which are represented by δ and Ω terms in the expressions of H_1. Our aim of the present study is to examine the effect of γ, δ, and Ω on the superfluid order parameters. Below we explain our plan presentation.

In Sec. II, we begin by giving a detailed analysis of the mean-field procedure and obtain the phase diagram for MI-SF transition in the t-μ plane for representative values of γ for zero and finite values of the detuning field δ. Following this, we look into the phases and magnitudes of the SF order parameter in a superfluid regime. We show that the phases and the magnitudes of the SF order parameters respond differently as the parameters are varied. We find that when $t/\gamma \gg 1$, the SF phase is described by a homogeneous superfluid where the magnitudes and the phases of the SF order parameter are spatially uniform. For intermediate values where $t \sim \gamma$, we find that the phases and the amplitudes of both species of the SF order parameter are inhomogeneous and show a large vortexlike pattern. Depending on the relative strength of t and γ, it could be the superposition of local homogeneous phases and patches where the phases form a spiraling pattern. For the limit $t/\gamma \ll 1$, the phases of the order parameter develop a ferromagnetic order along the diagonal direction followed by periodic modulations of magnitude of the SF order parameter. We explain that this is due to inherent frustration brought in by the spin-orbit interaction. The gradual transition of the phase textures for $t/\gamma \gg 1$ to $t/\gamma \ll 1$ is possibly a crossover phenomena where, due to the presence of spin-orbit coupling term γ, the phases begin to fluctuate from a homogeneous distribution and reach an ordered pattern via a disordered intermediate regime. The scenarios could be described as ordered-disordered-ordered phenomena. In Sec. III, we discuss the effect of detuning field δ on the distribution of phases and the magnitude of the SF order parameter. We find that it brings in additional correlation between the phases of the SF order parameter of two species.

In Sec. IV, we study the fluctuations around the mean-field configuration and investigate the lowest possible excitations. In Sec. V, we study the dynamics of phases inside the deep SF regime. Assuming that the phases of the order parameters are the only relevant low-energy degrees of freedom in this regime, we deduce the Euler-Lagrange equation of motion for it and find the normal modes of small oscillations. It appears that, due to the constrained collective motions among the phases of the nearest-neighbor bosons, imaginary frequency appears signifying damped vibration. We also look at the nature of lowest normal modes of the vibrations. The density distribution and the rich phase textures we obtain due to interplay of various system parameters (i.e., t,γ,δ) could be experimentally detected by possible noise-correlation measurement, mass current measurement, and the presence of additional peaks in Bragg scattering or *in situ* microscopy [32–34]. We summarize our work in Sec. VI.

II. MEAN-FIELD STUDY

As already mentioned, in this work we study spin-orbit-coupled two component bosons in square lattice described by the Hamiltonians in Eq. (1). Our primary purpose is to examine how the phase and the magnitude of the SF order parameter behave as various system parameters are changed. In our analysis all the parameters have been scaled by the on-site spin-independent density-density interaction U. To begin with we keep the on-site detuning parameter $\delta = 0.0$. The effect of δ has been discussed in Sec. III. We confine our numerical results for a system of size 10×10. In all cases, the chemical potential μ is taken to be 0.2 and interspecies interaction strength λ is fixed at 0.6. For our purpose of mean-field analysis we take the Gutzwiller variational wave function as $|\Psi\rangle = \prod_i |\psi_i\rangle$, where $|\psi_i\rangle$ is the wave function at a given site i. $|\psi_i\rangle$ is given by $|\psi_i\rangle = \sum_{m,n} f_{m,n}|mn\rangle$. Here $|mn\rangle$ denotes a state with m (and n) boson(s) of species 1 (and 2). f_{mn} is the Gutzwiller coefficient associated with the state $|mn\rangle$. As we work in a strong-coupling limit where U is much larger that t and γ and other system parameters, it is sufficient to take states up to two particles at a given site. The mean-field superfluid order parameters are defined as $\Delta_{ia} = \langle\psi_i|b_{ia}|\psi_i\rangle$; here i denotes the site index and a signifies the species index which could take values 1 and 2. A nonzero value of Δ_{ia} indicates a superfluid phase. The expressions for Δ_{ia} in terms of $f_{mn,i}$ are given below:

$$\begin{aligned}\Delta_{i1} &= f_{10,i}f_{00,i}^* + f_{11,i}f_{01,i}^* + \sqrt{2}f_{20,i}f_{10,i}^*,\\ \Delta_{i2} &= f_{01,i}f_{00,i}^* + f_{11,i}f_{10,i}^* + \sqrt{2}f_{02,i}f_{01,i}^*.\end{aligned} \tag{2}$$

The first part of the Hamiltonian in Eq. (1) excluding the hopping term contains on-site interactions and we call it H_{at}. The expectation value of it with respect to Gutzwiller

variational wave function $|\Psi\rangle$ is given by

$$\begin{aligned}\langle H_{at}\rangle_i = &-\mu_1(|f_{10,i}|^2+|f_{11,i}|^2+2|f_{20,i}|^2)+\lambda U|f_{11,i}|^2\\ &-\mu_2(|f_{01,i}|^2+|f_{11,i}|^2+2|f_{02,i}|^2)\\ &+2U(|f_{20,i}|^2+|f_{02,i}|^2).\end{aligned} \tag{3}$$

Here $\langle H_{at}\rangle_i$ denotes contribution from ith site in H_{at}. A generic term in H_1 [and the spin-independent hopping term in Eq. (1)] can be written as $b^\dagger_{i,\alpha}b_{j,\beta}$. The mean-field decomposition of it is given by [27,31]

$$b^\dagger_{i,\alpha}b_{j,\beta} = \Delta^*_{i\alpha}b_{j\beta}+\Delta_{j\alpha}b^\dagger_{i\beta}-\Delta^*_{i\alpha}\Delta_{j\beta}, \tag{4}$$

where Δ_{ia} is the mean-field order parameter as evaluated in Eq. (2). After we substitute Eqs. (3) and (4) in Eq. (1), and use Eq. (2) we can write the mean-field decomposed Hamiltonian as

$$H = \sum_i \chi_i^\dagger F_i(\mu,\lambda,\Delta_{j,\alpha},t,\gamma)\chi_i, \tag{5}$$

where $\chi_i^\dagger = (f_{00,i}, f_{10,i}, f_{01,i}, f_{11,i}, f_{20,i}, f_{02,i})$. The problem then reduces to diagonalizing the matrix F_i at every site self-consistently. In the Appendix, we have given the full expression of the matrix F_i in Eq. (A1). The Hamiltonian in Eq. (5) is still a coupled problem as it involves the order parameters of nearest-neighbor sites. We notice that, in the presence of spin-orbit coupling, $\Delta_{i\alpha}$ cannot be taken uniform at each site as in that case the spin-orbit interaction contributes nothing to the total energy. To find the mean-field solution, we start from a given random initial distribution of $\Delta_{i\alpha}$ at each site i and diagonalize the $F_i(\mu,\lambda,\Delta_{j,\alpha},t,\gamma)$ at each site. We then calculate the new set of $\tilde{\Delta}_{i\alpha}$ corresponding to the minimum eigenvalue of F_i. The resulting $\tilde{\Delta}_{i\alpha}$'s are fed back into Eq. (5) until Δ_i becomes equals to $\tilde{\Delta}_i$ at each site i. We do this procedure for approximately 10^3 random configurations and take the configurations of $\tilde{\Delta}_{i\alpha}$ which corresponds to the global minima. In the left panel of Fig. 1, we show the phase diagram for the MI-SF transitions in the t-μ plane for representative values of γ with $\delta = 0.0$. In the right panel of Fig. 1, we have plotted the MI-SF transition for $\delta = 0.005$. We notice that the results shown in Fig. 1 match well with the earlier results in Refs. [18,20]. Now we discuss the phases and the magnitudes of the SF order parameters for different values of t and γ.

A. Numerical results

We have found, in general, that the presence of spin-orbit coupling (γ) in two species bosons as given in Eq. (1) yields an inhomogeneous superfluid phase where the phases of the superfluid order parameter are spatially nonuniform. When the spin-conserved hopping parameter (t) dominates over spin-orbit coupling γ, then the superfluid phase could be described as a homogeneous superfluid phase but when γ is comparable to t or larger than t, the phases and the magnitudes of the SF order parameters are not homogeneous and in general show different behavior depending on the relative strength of t and γ. First we discuss the regime when $t \gg \gamma$, followed by the regime where $t \sim \gamma$. After this we discuss the regime where $\gamma \gg t$.

1. When $t/\gamma \gg 1$

In Fig. 2, we present the resulting distributions of phases and the magnitude of the order parameter $\Delta_{i\alpha}$. The arrows represent the phases and the background color represents the relative magnitudes of the order parameters. The dark color represents greater magnitude. The upper panel is for Δ_{i1} and the lower panel is for Δ_{i2}. In the extreme left panel the result is shown for $t = 0.04, \gamma = 0.02$. We find that the distribution of phases Δ_{i1} are ordered and spatially uniform, while that of Δ_{i2} is disordered. The magnitudes of Δ_1 form a two sublattice structure; however, there are degenerate solutions with spatially uniform magnitude. It is clear that the two sublattice structure is the result of spin-orbit interaction. Also we have $\langle\Delta_{i1}\rangle \gg \langle\Delta_{i2}\rangle$. The above differences in phase and amplitude distribution between the two species are due to the presence of Ω; the system is favoring the condensation of species 1 which resembles the homogeneous superfluid. The middle panel of Fig. 2 represents the result for $t = 0.04, \gamma = 0.025$. We observe that the phases of the superfluid order parameter are no longer uniform in space and change from one position to another having a definite twist angle between them, leading to what has been called a twisted superfluid phase [22]. We observe the reduction of the ordered pattern of Δ_{i1} and

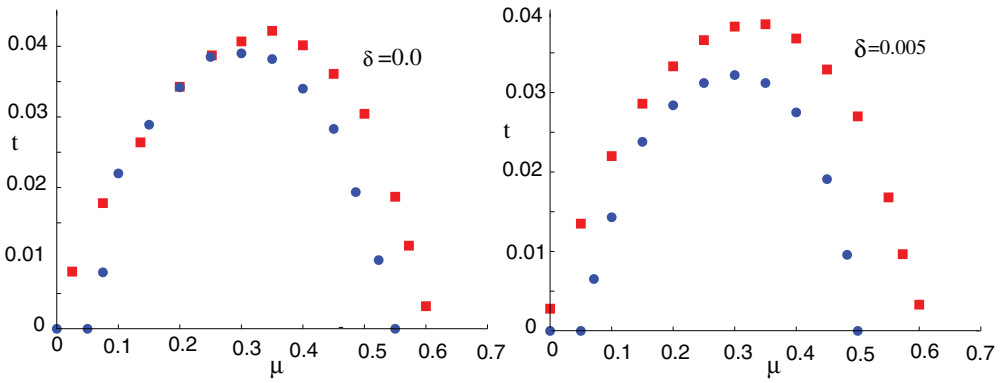

FIG. 1. (Color online) Here we have shown the MI-SF transition in the t-μ plane. In the left panel we have shown the MI-SF transition for $\delta = 0.0$ and the right panel is for $\delta = 0.005$. The red points denote the transition for $\gamma = 0.0$ and the blue points denote the transition for $\gamma = 0.04$. For both panels λ is 0.6 and Ω is 0.01.

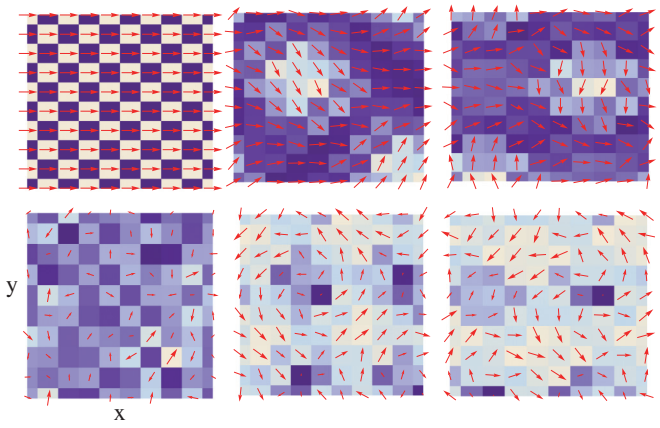

FIG. 2. (Color online) Small square boxes containing arrows denote the positions of a site in a 10×10 square lattice. The distance from lower horizontal boundary and the distance from left vertical boundary gives, respectively, the (x,y) coordinates in the usual Cartesian coordinate system. This description goes for Figs. 3–6, 9, and 10. Magnitude and phase of the order parameter is plotted at each site. The arrows represent the phases and the color represents the magnitude of the order parameter Δ_i. The upper panel denotes phase and magnitude for Δ_1 and the lower panels are for Δ_2. The left panels denote the result for $\gamma = 0.02, t = 0.04$. The middle panels are for $\gamma = 0.025, t = 0.04$ and the right panels are for $\gamma = 0.03, t = 0.04$. We have set $\Omega = 0.01$. In these figures and the subsequent figures dark color represents greater amplitude and white color means lesser amplitude but never zero. The color scheme used in different figures is to be compared qualitatively only.

onset of diagonal ordering. Interestingly, we observe that whenever the phase of the SF order parameter Δ_{i1} is deviated from zero (indicated by horizontal alignment of arrows), it is accompanied with a reduction of the magnitudes of the order parameter. The phases of Δ_{i2} also show signature of diagonal ordering. The competition between ordering along the two diagonal directions result in forming large vortices as seen in the middle lower panel in Fig. 2. The right panels of Fig. 2 represents the results for $t = 0.04, \gamma = 0.03$. In all the cases we have taken $\Omega = 0.01$.

2. *When $t \sim \gamma$*

The phase textures for this regime could be described as follows. We find a competition between local ferromagnetic alignment for the nearest Δ_i's and the ferromagnetic (FM) ordering along the diagonal neighbors. The FM ordering for the neighboring sites results from direct hopping, whereas the ferromagnetic ordering along the diagonal sites is due to the spin-orbit coupling as explained in next section. In Fig. 3, the left panel represents the phase distribution for $\gamma = 0.035$, the middle panel is for $\gamma = 0.04$, and the right panel is for $\gamma = 0.06$. For all figures in Fig. 3 the value of t is also set at 0.04. We notice that the minimum-energy configuration presented here is not unique. There are many degenerate configurations with identical energy. However, the quantum fluctuations would pick up the global minima. For example, in Fig. 3, we find the onset of density modulations and no vertex formations. There are degenerate mean-field

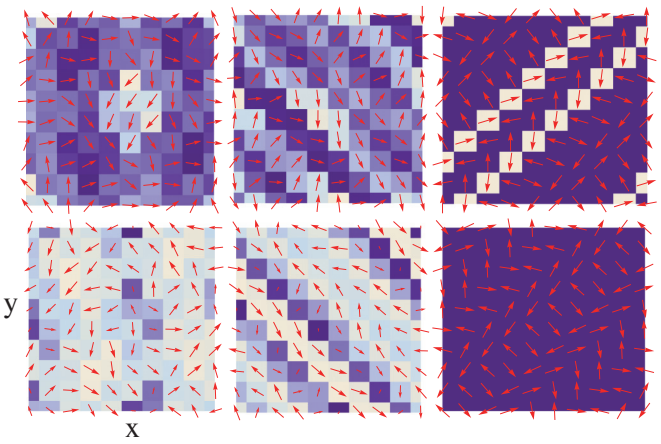

FIG. 3. (Color online) Distribution of phase and the order parameter as explained in Fig. 2. Here the left panels represent the result for $\gamma = 0.035, t = 0.04$, the middle panels represent $\gamma = 0.04, t = 0.04$, and the right panels represent $\gamma = 0.06, t = 0.04$. We have taken $\Omega = 0.01, \delta = 0.0$.

solutions with completely random density distribution with isolated vertex formations.

3. *When $t/\gamma \ll 1$*

In this regime we notice that the phases form a ferromagnetic alignment along any one of the diagonals. The magnitude of the order parameter is also seen to be modulated. In Fig. 4, we present the distribution for the phases and the magnitudes of SF order parameter for $\gamma = 0.1, t = 0.02$. We see that ferromagnetic ordering of phases along the diagonal is fully established. While in the left panel FM ordering happens for both diagonals, for the middle panel it happens for only the (1,1) direction. In the left panel isolated vertex

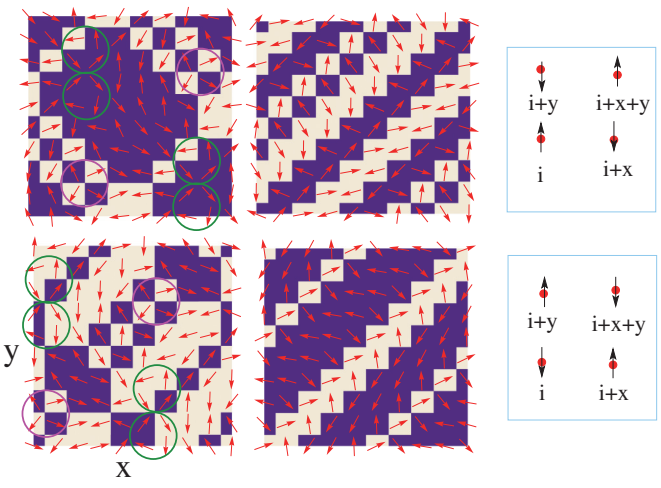

FIG. 4. (Color online) Distribution of phases and the order parameter as explained in Figs. 2 and 3. The left and the middle panel are drawn for $\gamma = 0.1, t = 0.02$. We have kept $\Omega = 0.01, \delta = 0.0$. These represent the degenerate mean-field configuration. We see that the left panel contains vertex and antivertex. The green circle contains the vertex configurations and the pink circle contains antivertex. In the right panel we have shown the spin-orbit-coupled hopping processes for up-spin starting from site i in the counterclockwise direction.

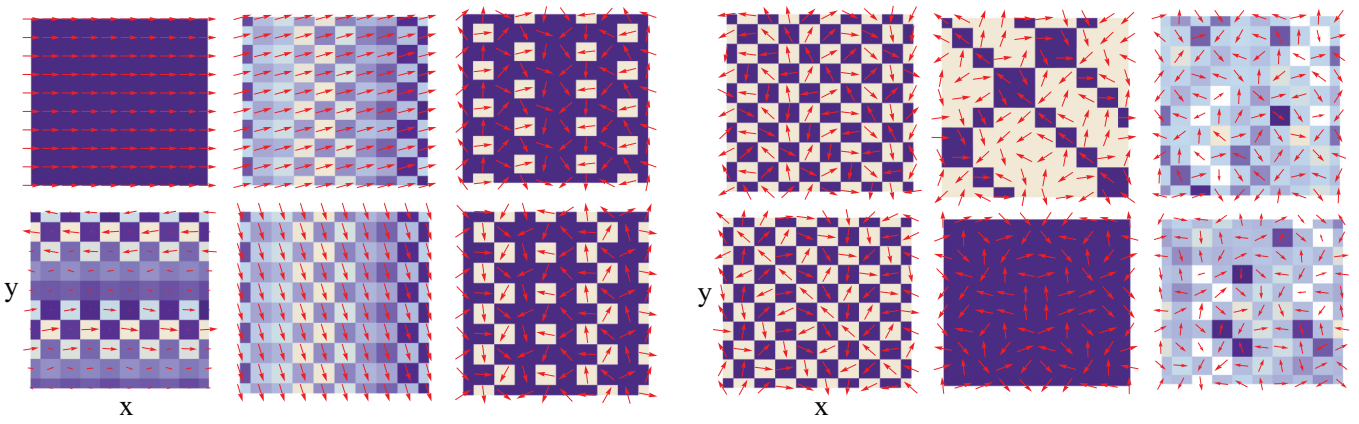

FIG. 5. (Color online) (Left) Distribution of phases and amplitude for $\delta = 0.005$. The values of t,γ for the left panel are (0.04, 0.02), for the middle panel (0.04, 0.025), and for the right panel (0.04, 0.03). (Right) Distribution of phases and amplitude for $\delta = 0.005$. The values of t,γ for the left panel are (0.04, 0.035), for the middle panel (0.04, 0.04), and for the right panel (0.04, 0.06). For all the figures, the values of μ,λ are respectively 0.2 and 0.6.

[11] and antivertex is seen to appear. To understand the phase distribution in this regime it may be useful to consider an elementary square plaquette and consider the meanfield Hamiltonian for it. Let us consider the hopping of an up spin under spin-orbit coupling via the sites i, $i+x$, $i+x+y$, and $i+y$ in a counterclockwise direction as shown in the right upper panel in Fig. 4. The mean-field decomposition of the Hamiltonian for the bonds of an elementary square shown in the right panel of Fig. 4 imposes the following constraints on the phases:

$$\begin{aligned} \theta_{i,1} - \theta_{i+x,2} = \pm\pi, \quad \theta_{i+x,2} - \theta_{i+x+y,1} = \frac{\pi}{2}, \\ \theta_{i+x+y,1} - \theta_{i+y,2} = 0, \quad \theta_{i+y,2} - \theta_{i,1} = -\frac{\pi}{2}. \end{aligned} \tag{6}$$

In the above $\theta_{j\alpha}$ denotes the phases of the SF order parameter $\Delta j\alpha$. The above set of equations does not have simultaneous solutions for all the parameters. One may eliminate $\theta_{i+x,2}$ (and $\theta_{i+y,2}$) from the first and second (and third and fourth) to solve for $\theta_{i,1}$ and $\theta_{i+x+y,1}$ to obtain that they are equal. The numerical results seem to confirm this. It then poses an ill-defined equation for $\theta_{i+x,2}$ (and $\theta_{i+y,2}$) which is fixed to minimize the palette energy. The ratio of average palette energy obtained from numerics to that obtained by minimizing a single plaquette is 0.94, which is satisfactory. In recapitulation, we have shown within the mean-field how the twisted superfluid phase appears as we gradually tune the parameter t and γ for a tight-binding Hamiltonian given in Eq. (1). We have shown the onset of density modulations and stripe pattern [35,36] for the phases as γ is increased gradually. The transition of the phase textures for $t/\gamma \gg 1$ to $t/\gamma \ll 1$ is possibly a crossover phenomena where, due to the presence of spin-orbit-coupling term γ, the phases start to fluctuate from a homogeneous distribution and reach an ordered pattern via a disordered intermediate regime. The scenarios could be described as ordered-disordered-ordered phenomena.

III. EFFECT OF FINITE δ

Here we discuss the effect of detuning field δ. We find that for very small values of δ the resulting phase and amplitude distribution does not differ from the case $\delta = 0.0$. However, as we increase δ, it starts to effect the resulting phase and amplitude distribution of the SF order parameter in a significant and distinctive way. In Fig. 5, we have shown the results for $\delta = 0.005$. We have observed that for $\gamma = 0.02, t = 0.04$, as shown in the left panel of Fig. 5, the nature of the phase distribution does not change from that of the $\delta = 0.0$ case as shown in the left panel of Fig. 2. However, for $\gamma = 0.025, t = 0.04$, we observe that finite δ has brought in substantial differences from that of the $\delta = 0.0$ case. For these parameter values $\delta = 0.0$ has already initiated a twisted superfluid phase; however, for finite δ we observe a uniform superfluid phase as seen in the middle panel of the left of Fig. 5. But we find that though the phase distribution of both the species of bosons are uniform, the relative phase difference between two species is 90° due to the presence of δ. This feature continues for small to medium values of γ as described in Fig. 5. For $\gamma = 0.03$ we observe that a twisted superfluid phase has appeared but for a given site the phases of two species of bosons are at 90°. This feature may be explained in the following way. The detuning term at a given site is given by $\delta(ib_1^\dagger b_2 + \text{H.c.})$ (we have omitted the site index i), which yields a mean-field decomposition $\sim 2\delta|\Delta_1||\Delta_2|\sin(\theta_1 - \theta_2)$. The appearance of $\sin(\theta_1 - \theta_2)$ brings in additional correlations between the phases of two species at a given site i. When γ is small, the detuning term maximizes itself by making $\theta_1 - \theta_2 = 90°$. For this reason we find that the resulting phase distribution is distinctively different from that of $\delta = 0.0$. The diagonal ordering that was very strong for the $\delta = 0.0$ case is not that prominent for $\delta = 0.005$ due to the additional competing mechanism brought in by δ. However, for very large values of γ as shown in the right panel of Fig. 6, we find that the effect of δ has been minimized and the diagonal ordering has been fully established similar to the $\delta = 0.0$ case. So far, we have discussed the effect of δ on the phases of the order parameter. The effect of the detuning parameter δ acts as a leveler as far as the amplitude of the order parameter is concerned. We have observed that for $\gamma \ll t$ and $\gamma \sim t$ the amplitude of Δ_{i1} and Δ_{i2} are same. Though in Fig. 5 we see differences in the amplitudes of Δ_1 and Δ_2, they differ in the sixth decimal

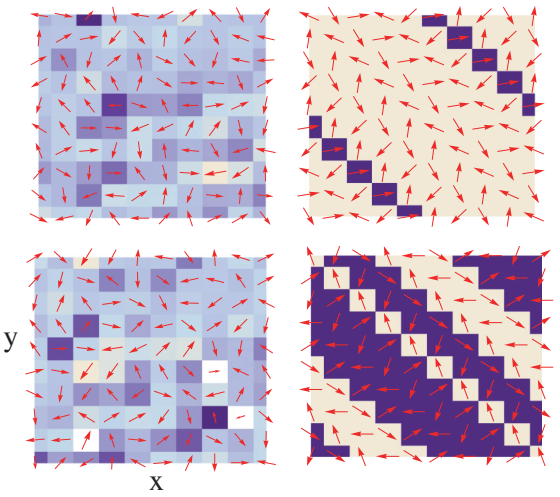

FIG. 6. (Color online) (Right) Distribution of phases and amplitude for $\delta = 0.005$. The values of t,γ for the left panel are (0.04, 0.08) and for the right panel (0.02, 0.1). For all the figures, the values of μ,λ are respectively 0.2 and 0.6.

places implying that they are almost equal. However, for $\gamma \gg t$ (presented in Fig. 6), we see that the magnitudes of Δ_{i1} and Δ_{i2} differ and form a modulated pattern. Thus we conclude that sufficiently strong values of the detuning parameter δ bring in distinct differences on the phase and amplitude distributions of the SF order parameters when compared to the $\delta = 0$ case.

IV. FLUCTUATION AROUND THE MEAN FIELD

Having discussed the phase and amplitude distribution for different values of t and γ within the mean field, we now look into the fluctuations around the mean-field solutions obtained in the previous sections. We confine our analysis for the $\delta = 0.0$ case as the small but finite δ is seen to yield no new feature in the fluctuations. To take into account the role of fluctuations, we expand the Gutzwiller coefficient [37] $f_{mn,i}$ around its mean-field value and expand it as $f_{mn,i} = \bar{f}_{mn,i} + \delta f_{mn,i}$, where $\bar{f}_{mn,i}$ represents the mean-field value. After we substitute it in Eq. (5) we retain the terms which are quadratic in $\delta f_{mn,i}$ (and its complex conjugate). The resulting Hamiltonian then could be written as

$$H = \Psi^{\dagger} H_{\delta} \Psi. \tag{7}$$

Here $\Psi^{\dagger} = (\psi_1, \psi_2, \ldots, \psi_r, \ldots, \psi_N)$ and $\psi_i = (\psi_{ui}, \psi_{di})$. Here $\psi_{ui} = (\delta f_{00,i} \delta f_{10,i} \delta f_{01,i} \delta f_{11,i} \delta f_{20,i} \delta f_{02,i})$ and $\psi_{di} = \psi^*_{ui}$. It is clear that H_{δ} represents a $12N \times 12N$ Hermitian matrix whose eigenvalues and eigenvectors represent the collective modes. It may be noted that the substitution, $\delta f_{mn,i} = \sum_k u_{mn,k} e^{ikr} + v_{mn,k} e^{-ikr}$, does not simplify the calculation as the $\bar{f}_{mn,i}$'s are not translational invariant. We denote the lowest positive eigenvalue by E_0 (10^{-16}). The E_0 is a measure of possible low-energy collective modes of the system and is shown in Fig. 7. In the left panel of Fig. 7, $\log_{10} E_0$ has been plotted with N as the system size. The various colors represent various sets of parameters (γ,t). Red represents (0.1, 0.02), blue represents (0.02, 0.04), green represents (0.03, 0.04), black is for (0.04, 0.04), gray is for (0.06, 0.04), orange denotes (0.08, 0.04), magenta denotes (0.025, 0.04), and cyan

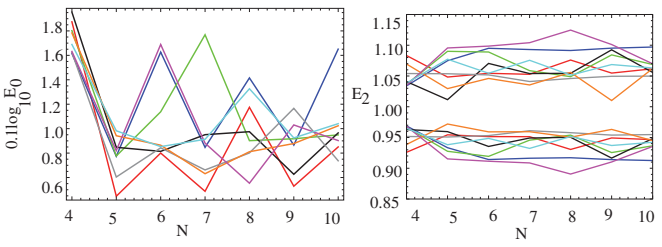

FIG. 7. (Color online) In the left panel a measure of zero energy eigenmodes, E_0, due to the collective motions has been shown. In the right panel the bandwidth around E_2 has been plotted. For both, the figure horizontal axis represents the length of a $N \times N$ lattice. The various colors represent various sets of parameters as described in the text.

is for (0.035, 0.04). This color scheme is maintained for all the figures that will be used later. In the following we discuss the textures of the order parameter Δ_{ia} for different values of t and γ. We find that for $t \gg \gamma$, the system always find zero energy modes. For $t \sim \gamma$, where the phases are disordered, we also find similar behavior. However, for $\gamma \gg t$, we find that E_0 is $\sim 10^4$ times larger than the other parameter regime. However, E_0 scales to lower values monotonically as we increase the system size. The gradual decrease of E_0 with system size N indicates that it is approaching the possible zero-energy modes. The reason that, for $\gamma \gg t$, E_0 is larger than other cases by a few thousand order is the following. For $t \gg \gamma$ the uniform phase distribution always find nearly zero-energy collective modes and there is no frustration in the system also. For $t \sim \gamma$, the spins are disordered and random. Thus it is easily possible to redistribute the phases to have low-energy eigenmodes which are nearly degenerate with the original solutions. However, for $\gamma \gg t$, the distribution of phases and the magnitudes are determined by the frustration brought in by spin-orbit coupling. The degenerate solutions in this case as seen from Fig. 4 are not easily connected. Thus the lowest possible collective excitations cost more energy than other cases. However, as we increase the system size, we expect that the degenerate solutions are easily obtained from one another leading to nearly zero-energy excitations. We also observe that the eigenvalues of the collective modes form three distinct bands. This is clear from Eq. (3). The fluctuation of $f_{2,0}$ or $f_{0,2}$ yields the bands around U, while the fluctuation of f_{11} yields the bands around $\lambda/2$. The fluctuation of $f_{1,0}$, $f_{0,1}$, and $f_{0,0}$ constitutes the lower bands. We denote these three bands by E_2, E_1, and E_0, respectively. In the right panel of Fig. 8, we have plotted the

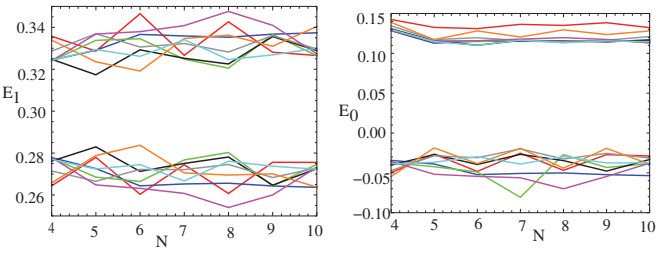

FIG. 8. (Color online) In the left panel the bandwidth around E_1 has been shown. The right panel is for E_0. In both the figures the horizontal axis represents the length of a $N \times N$ lattice.

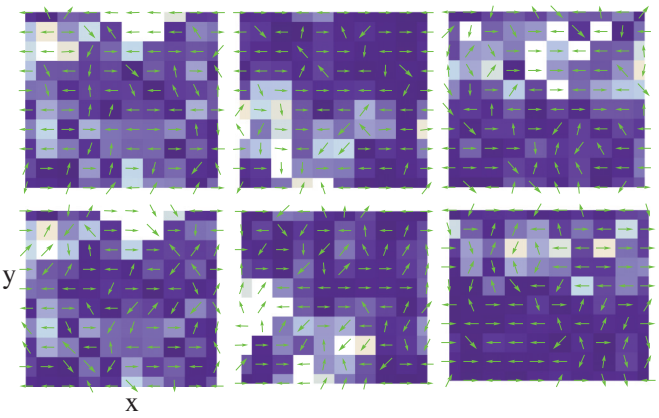

FIG. 9. (Color online) Magnitude and phase of the order-parameter fluctuation are plotted at each site. The arrows represent the phases and the color represents the magnitude of the order-parameter fluctuation δ_i. The upper panel denotes phase and magnitude for δ_1 and the lower panels are for δ_2. The left panels denote the result for $\gamma = 0.025, t = 0.04$. The middle panels are for $\gamma = 0.04, t = 0.04$ and the right panels are for $\gamma = 0.1, t = 0.02$. As mentioned, we have taken $\mu = 0.2, \lambda = 0.6, \delta = 0.0$.

bandwidth with the system sizes for different parameter values. In the left panel of Fig. 8 we have plotted the bandwidth formed around E_1 and the right panel is for around E_0. It appears that, for a given t, the bandwidth is inversely proportional to γ. Also, the greater the value of γ, the more the bandwidth oscillates with the system sizes. We notice that the bands E_2 and E_1 are symmetric but E_0 is not because of the presence of Ω.

In Fig. 9 we have represented the fluctuation of the order parameter $\Delta_{i\alpha}$. By expanding $f_{mn,i}$ around its mean-field value $\bar{f}_{mn,i}$ we can express $\Delta_{i,a} = \bar{\Delta}_{i,a} + \delta_{i,a}$, where $\delta_{i,a}$ is given below:

$$\begin{aligned}\delta_{i,1} &= \bar{f}_{10,i}\delta f^*_{00,i} + \bar{f}^*_{00,i}\delta f_{10,i} + \delta f_{10,i}\delta f^*_{00} \\ &\quad + \bar{f}_{11,i}\delta f^*_{01,i} + \bar{f}^*_{01,i}\delta f_{11,i} + \delta f_{11,i}\delta f^*_{01,i} \\ &\quad + \sqrt{2}(\bar{f}_{20,i}\delta f^*_{10,i} + \bar{f}^*_{10,i}\delta f_{20} + \delta f_{20,i}\delta f^*_{10}), \\ \delta_{i,2} &= \bar{f}_{01,i}\delta f^*_{00,i} + \bar{f}^*_{00,i}\delta f_{01,i} + \delta f_{01,i}\delta f^*_{00} \\ &\quad + \bar{f}_{11,i}\delta f^*_{10,i} + \bar{f}^*_{10,i}\delta f_{11,i} + \delta f_{11,i}\delta f^*_{10,i} \\ &\quad + \sqrt{2}(\bar{f}_{02,i}\delta f^*_{01,i} + \bar{f}^*_{01,i}\delta f_{02} + \delta f_{02,i}\delta f^*_{01}).\end{aligned} \tag{8}$$

$\delta f_{mn,i}$'s has been calculated from the eigenvectors corresponding to E_0. Using the values of $\delta f_{mn,i}$ we calculate $\delta_{i,a}$ according to Eq. (8). Its magnitude and phases have been plotted in Fig. 9. This yields the probable low-energy collective modes for the finite-size system. We observe quite distinct patterns in three different limits. For $t/\gamma \gg 1$, we find that the fluctuation of magnitude of $\delta_{i,1}$ is $\delta_{i,2}$ follows each other. The phase fluctuation is such that it is almost an equal superposition of parallel and antiparallel phases so that the sum, $\sum_{i,j} \cos(\theta_i - \theta_j) \sim 0.0$, is given in horizontal or vertical line. For some nearest-neighbor bonds, the phases are right angles contributing $\cos(\theta_i - \theta_j) \sim 0.0$. The phase fluctuation of δ_2 follows a similar pattern as in $\delta_{i,1}$, though deviations are seen due to the presence of γ. For the cases $t/\gamma \sim 1$ and $t/\gamma \ll 1$, we find a diagonal ordering which is broken at midway by opposite alignment of phases at the nearest diagonal sites. Also we notice that the fluctuation of the magnitudes of $\delta_{i,1}$ and $\delta_{i,2}$ start to deviate slowly as we increase the value of γ.

V. DYNAMICS OF THE PHASES

Now we turn our attention to deep inside the superfluid regime where one may neglect the fluctuations of the magnitude of the order parameter and consider the phases as the only relevant degree of freedom. Following a semiclassical approximation, we deduce the Lagrangian and the equation of motion for the phases and determine the normal modes of the vibrations. For simplicity, we have taken $\delta = 0.0$ in the following analysis. The mean-field decomposition of Eq. (1) could be written as

$$\begin{aligned}H &= \sum_i \mu_{\alpha,i}\langle n_{\alpha,i}\rangle + \frac{U}{2}\langle n_{\alpha,i}\rangle^2 + \lambda U\langle n_{\alpha,i}\rangle\langle n_{\beta,i}\rangle \\ &\quad - \sum_{\langle ij\rangle}(\lambda_{ij,\alpha\beta}\Delta^*_{\alpha,i}\Delta_{\beta,j} + \text{H.c.}).\end{aligned} \tag{9}$$

In the above $\lambda_{ij,\alpha\beta}$ denotes a generalized hopping parameter. The main disadvantage of Eq. (9) is that all the variables commute with each other and bear no signature of the original bosonic commutation relations. To derive the Lagrangian of the phases of the order parameter $\Delta_{i\alpha}$, we follow the procedure in [38,39]. Translating the original bosonic commutators to the commutation relations of the mean-field variables, we find that

$$[n_1, b_1] = -b_1 \rightarrow [\langle n_1\rangle, \Delta_1] = -\Delta_1. \tag{10}$$

Writing $\Delta_1 = e^{i\theta_1}|\Delta_1|$ and keeping $|\Delta_1|$ constant we obtain

$$[\langle n_1\rangle, e^{i\theta_1}] = -e^{i\theta_1}. \tag{11}$$

Expanding $e^{i\theta_1}$ and keeping only the lowest-order term we obtain, for $\theta_1 \rightarrow 0$, the following commutation relations:

$$[\langle n_1\rangle, \theta_1] = i, \quad [\langle n_1\rangle^2, \theta_1] = 2i\langle n_1\rangle. \tag{12}$$

The above procedure yields the following coupled equations involving $\frac{\partial\theta_\alpha}{\partial t}$ and $\langle n_{\alpha i}\rangle$:

$$\begin{aligned}\frac{\partial\theta_{1i}}{\partial t} &= -\left(\mu + \Omega + \frac{U}{2}\right) + U\langle n_{1i}\rangle + \lambda U\langle n_{2i}\rangle, \\ \frac{\partial\theta_{2i}}{\partial t} &= -\left(\mu - \Omega + \frac{U}{2}\right) + U\langle n_{2i}\rangle + \lambda U\langle n_{1i}\rangle.\end{aligned} \tag{13}$$

Solving for $\langle n_{1i}\rangle$ and $\langle n_{2i}\rangle$ from the above two equations and substituting in the Hamiltonian in Eq. (9), we obtain the following equations:

$$\begin{aligned}H_{sh} &= B_0\left[\left(\frac{\partial\theta_{1i}}{\partial t}\right)^2 + \left(\frac{\partial\theta_{2i}}{\partial t}\right)^2\right] + B_1\frac{\partial\theta_{1i}}{\partial t} + B_2\frac{\partial\theta_{2i}}{\partial t} \\ &\quad + B_3\frac{\partial\theta_{1i}}{\partial t}\frac{\partial\theta_{2i}}{\partial t} + \tilde{F}(\theta_{i1},\theta_{i2}) + B_4,\end{aligned} \tag{14}$$

where $\tilde{F}(\theta_{i1},\theta_{i2})$ is given in the Appendix. Expressions for B_i's are also given in the Appendix. To derive the Euler-Lagrange equations of motion, we introduce the relative and total phase by the relation $\theta_{1i} = \theta_{ci} + \theta_{ir}, \theta_{2i} = \theta_{ci} - \theta_{ir}$. After inserting the above change of variables, we can rewrite Eq. (14) as

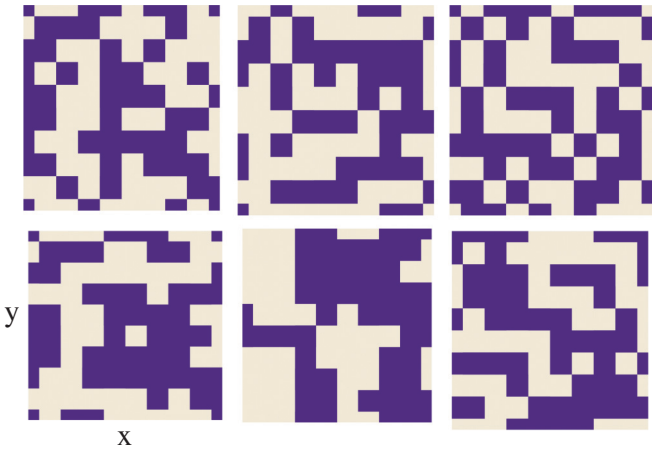

FIG. 10. (Color online) We have shown the nature of vibration for the lowest normal modes. In each panel the upper panels denote vibrations of θ_1 and the lower panels are for θ_2. The right panel denotes the case $\gamma < t$ ($\gamma = 0.02, t = 0.04$). The middle panel represents $\gamma \sim t$ ($\gamma = 0.04, t = 0.04$). The right panel represents $\gamma > t$ ($\gamma = 0.1, t = 0.02$). As mentioned, we have taken $\mu = 0.2, \lambda = 0.6, \delta = 0.0$. The white region denotes motion in the clockwise direction and the blue region denotes motion in the counterclockwise direction.

follows:

$$H_n = \sum_i T_1(\dot{\theta}_{ic} + \alpha_c)^2 + T_2(\dot{\theta}_{ir} + \alpha_r)^2 + \tilde{F}(\theta_{ir}, \theta_{ic}) + \sum \alpha_{icr}. \tag{15}$$

Here $T_{1/2} = 2B_0 \pm B_3$. Using the above equations, we write the resulting Lagrangian and the equation of motion below:

$$\mathcal{L} = \sum_i T_1(\dot{\theta}_{ic} + \alpha_c)^2 + T_2(\dot{\theta}_{ir} + \alpha_r)^2 - \tilde{F}(\theta_{ir}, \theta_{ic}),$$
$$\ddot{\theta}_{ic} = -\frac{\partial \tilde{F}(\theta_{ic}, \theta_{ir})}{T_1 \partial \theta_{ic}}, \quad \ddot{\theta}_{ir} = -\frac{\partial \tilde{F}(\theta_{ic}, \theta_{ir})}{T_2 \partial \theta_{ir}}. \tag{16}$$

In the last equation we have deliberately omitted the inconsequential constant term $\sum \alpha_{icr}$. After simplifying the right-hand side (RHS) of the second and third identity of Eq. (16) and subsequently expanding up to a linear term, we can rewrite it as $\ddot{\Theta} = M\Theta$, where, for a system of $N \times N$ lattice, Θ is a column matrix with $2N^2$ element such that $\Theta_i = \theta_{ic}$ and $\Theta_{N^2+i} = \theta_{ir}$ where i runs from 1 to N^2. M is a $2N^2 \times 2N^2$ square matrix. The eigenvalues of the matrix M yield the normal modes. We find that due to the presence of γ, the normal modes develop negative eigenvalues signifying damped modes. In Fig. 10 we have plotted schematically the lowest normal modes for three different regimes. In all the plots the blue region denotes displacements of phases in forward direction (counterclockwise rotation, $\theta_{1(2)}$ increasing) and the white regions denote displacements in the backward directions (clockwise rotation, $\theta_{1(2)}$ decreasing). The right panel denotes the case for $\gamma \gg t$, the middle panel denotes $\gamma \sim t$, and the right panel is for $t \gg \gamma$. In each of these panels the upper one denotes the displacement for species 1 and the lower panel describes the displacements for species 2. Looking at the upper panel we find that, for the $\gamma \gg t$, there is the tendency of phases to move synchronously along the diagonal which is expected. However, for the middle panel and the left panel there are preferences in horizontal ordering and patches of areas vibrating in breathing modes. For the species 2, as shown in the lower panel of Fig. 10, we find similar behavior though the region executing breathing modes is larger.

VI. DISCUSSION

To summarize, we have explored the different phases that might occur for spin-orbit-coupled bosons in the optical lattice in a strong-coupling limit. We have extensively studied the distribution of phases and the magnitude of the SF order parameter for a finite-size system using an inhomogeneous mean-field analysis. We have shown that for a given t, as we increase the spin-orbit interaction γ, we observe the destruction of the normal homogeneous superfluid phase and the onset of twisted superfluid phases. At large γ limit, a ferromagnetic ordering along the diagonal appears. Though our analysis was done for a finite-size system, this is possibly a crossover mechanism as explained in the text. We have also shown that the presence of δ brings in significant correlations between the phases of two species of bosons. We have also investigated the fluctuation around the mean field and discussed the nature of collective motions leading to possible zero-energy modes. The scaling of minimum-energy excitations with system size has also been shown. Finally, using semiclassical approximation, we derived the equation of motion for the phases and derive the normal modes of vibrations. We think that some of the results may have interesting experimental signatures in the light of recent experiments [32–34].

APPENDIX

The elements of the matrix $F_i(\mu, \lambda, \Delta_{j\alpha}, t, \gamma)$ are given below (for simplicity we shall not write the various parameters in the parentheses):

$$F_i = \begin{pmatrix} 0.0 & \Gamma_i & \tilde{\Gamma}_i & 0.0 & 0.0 & 0.0 \\ \Gamma_i^* & -(\mu+\Omega) & -i\delta & \tilde{\Gamma}_i & \sqrt{2}\Gamma_i & 0.0 \\ \tilde{\Gamma}_i^* & i\delta & -(\mu-\Omega) & \Gamma_i & 0.0 & \sqrt{2}\tilde{\Gamma}_i^* \\ 0.0 & \Gamma_i^* & \tilde{\Gamma}_i^* & -2\mu+\lambda U & i\sqrt{2}\delta & -i\sqrt{2}\delta \\ 0.0 & \sqrt{2}\Gamma_i^* & 0.0 & -i\sqrt{2}\delta & -2(\mu+\Omega)+2U & 0.0 \\ 0.0 & 0.0 & \sqrt{2}\Gamma_i^* & i\sqrt{2}\delta & 0.0 & -2(\mu-\Omega)+2U \end{pmatrix}. \tag{A1}$$

In the above $\Delta_{jx1(2)}$ denotes the up (down) contribution from two x neighbors, $\Delta_{jx1(2)} = \Delta_{i+x,1(2)} + \Delta_{i-x,1(2)}$. A similar explanation goes for $\Delta_{jy1(2)}$. Expressions for Γ_i and $\tilde{\Gamma}_i$ are

$$\Gamma_i = -t_1(\Delta^*_{jx1} + \Delta^*_{jy1}) + \gamma(\Delta^*_{jx2} + i\Delta^*_{jy2}),$$
$$\tilde{\Gamma}_i = -t_2(\Delta^*_{jx2} + \Delta^*_{jy2}) + \gamma(\Delta^*_{jx1} - i\Delta^*_{jy1}). \quad \text{(A2)}$$

Now we write down the expressions for B's and $\tilde{F}$ used in Sec. V:

$$B_0 = \frac{\lambda_0^2 U}{2}, \quad B_3 = u\lambda\lambda_0^2\left(1 - \frac{1}{\lambda^2}\right),$$

$$B_1 = \lambda_0\left(\frac{a_1}{\lambda} - a_2\right) + \lambda_0 U\left(A_2 - \frac{A_1}{\lambda}\right) + U\lambda\lambda_0\left(A_1 - \frac{A_2}{\lambda}\right),$$

$$B_2 = \lambda_0\left(\frac{a_2}{\lambda} - a_1\right) + \lambda_0 U\left(A_1 - \frac{A_2}{\lambda}\right) + U\lambda\lambda_0\left(A_2 - \frac{A_1}{\lambda}\right),$$

$$B_4 = -a_1 A_1 - a_2 A_2 + \frac{U}{2}\left(A_1^2 + A_2^2\right) + \lambda U A_1 A_2,$$

$$a_1 = \mu + \omega + \frac{U}{2}, \quad a_2 = \mu - \omega + \frac{U}{2}, \quad \lambda_0 = \frac{\lambda}{U(\lambda^2 - 1)},$$

$$A_1 = \lambda_0\left(a_2 - \frac{a_1}{\lambda}\right), \quad A_2 = \lambda_0\left(a_1 - \frac{a_2}{\lambda}\right), \quad \text{(A3)}$$

$$\alpha_c = \frac{B_1 + B_2}{2(2B_0 + B_3)}, \quad \alpha_r = \frac{B_1 - B_2}{2(2B_0 - B_3)},$$
$$\alpha_{icr} = -\alpha_c^2 - \alpha_r^2, \quad \text{(A4)}$$

$$\begin{aligned}\tilde{F}(\theta_{i1},\theta_{i2}) &= -2\gamma_t \sum_{\langle ij\rangle}[\cos(\theta_{1i} - \theta_{1j}) + \eta\beta^2\cos(\theta_{2i} - \theta_{2j})]\left|\delta_1^2\right| \\ &- 2\gamma_s\beta \sum_{\langle ij\rangle_x}[\cos(\theta_{2i} - \theta_{1jx}) - \cos(\theta_{1i} - \theta_{2jx})]\left|\delta_1^2\right| \\ &+ 2\gamma_s\beta \sum_{\langle ij\rangle_y}[\sin(\theta_{1i} - \theta_{2jy}) + \sin(\theta_{2i} - \theta_{1jy})]\left|\delta_1^2\right|. \quad \text{(A5)}\end{aligned}$$

[1] O. Morsch and M. Oberthaler, Rev. Mod. Phys. **78**, 179 (2006).
[2] J. Daliberd, F. Gerbier, G. Juzeliunas, and P. Ohberg, Rev. Mod. Phys. **83**, 1523 (2011).
[3] I. Bloch, J. Dalibard, and W. Zwerger, Rev. Mod. Phys. **80**, 885 (2008).
[4] M. Greiner, O. Mandel, T. Esslinger, T. W. Hansch, and I. Bloch, Nature (London) **415**, 39 (2002).
[5] C. Orzel, A. K. Tuchman, M. L. Fenselau, M. Yasuda, and M. A. Kasevich, Science **291**, 2386 (2001).
[6] G. Juzeliunas, J. Ruseckas, M. Lindberg, L. Santos, and P. Ohberg, Phys. Rev. A **77**, 011802(R) (2008); T. D. Stanescu, B. Anderson, and V. Galitski, *ibid.* **78**, 023616 (2008); X.-J. Liu, X. Liu, L. C. Kwek, and C. H. Oh, Phys. Rev. Lett. **98**, 026602 (2007).
[7] Y.-J. Lin, K. Jimnez-Garca, and I. B. Spielman, Nature (London) **471**, 83 (2011).
[8] X.-L. Qi and S.-C. Zhang, Rev. Mod. Phys. **83**, 1057 (2011).
[9] Y. A. Bychkov and E. I. Rashba, J. Phys. C **17**, 6039 (1984).
[10] G. Dresselhaus, Phys. Rev. **100**, 580 (1955).
[11] J. Radic, A. Di Ciolo, K. Sun, and V. Galitski, Phys. Rev. Lett. **109**, 085303 (2012).
[12] W. S. Cole, S. Zhang, A. Paramekanti, and N. Trivedi, Phys. Rev. Lett. **109**, 085302 (2012).
[13] Z. Cai, X. Zhou, and C. Wu, Phys. Rev. A **85**, 061605(R) (2012).
[14] R. Barnett, S. Powell, T. Grass, M. Lewenstein, and S. DasSarma, Phys. Rev. A **85**, 023615 (2012).
[15] C. Wang, C. Gao, C.-M. Jian, and H. Zhai, Phys. Rev. Lett. **105**, 160403 (2010).
[16] Y. Zhang, L. Mao, and C. Zhang, Phys. Rev. Lett. **108**, 035302 (2012).
[17] S. Sinha and K. Sengupta, Europhys. Lett. **93**, 30005 (2011); S. Powell, R. Barnett, R. Sensarma, and S. DasSarma, Phys. Rev. Lett. **104**, 255303 (2010); K. Saha, K. Sengupta, and K. Ray, Phys. Rev. B **82**, 205126 (2010).
[18] T. Grass, K. Saha, K. Sengupta, and M. Lewenstein, Phys. Rev. A **84**, 053632 (2011).
[19] A. Isacsson, M.-C. Cha, K. Sengupta, and S. M. Girvin, Phys. Rev. B **72**, 184507 (2005).
[20] S. Mandal, K. Saha, and K. Sengupta, Phys. Rev. B **86**, 155101 (2012).
[21] M. Killi, S. Trotzky, and A. Paramekanti, Phys. Rev. A **86**, 063632 (2012).
[22] P. Soltan-Panahi, D. Luhmann, J. Struck, P. Windpassinger, and K. Sengstock, Nat. Phys. **8**, 71 (2012).
[23] J. P. Vyasanakere, S. Zhang, and V. B. Shenoy, Phys. Rev. B **84**, 014512 (2011).
[24] M. P. A. Fisher, P. B. Weichman, G. Grinstein, and D. S. Fisher, Phys. Rev. B **40**, 546 (1989).
[25] S. Sachdev, *Quantum Phase Transitions* (Cambridge University Press, Cambridge, UK, 1999).
[26] D. Jaksch, C. Bruder, J. I. Cirac, C. W. Gardiner, and P. Zoller, Phys. Rev. Lett. **81**, 3108 (1998).
[27] K. Seshadri, H. R. Krishnamurthy, R. Pandit, and T. V. Ramakrishnan, Europhys. Lett. **22**, 257 (1993).
[28] M. Kruath and N. Trivedi, Europhys. Lett. **14**, 627 (1991).
[29] C. Trefzger and K. Sengupta, Phys. Rev. Lett. **106**, 095702 (2011).
[30] K. Sengupta and N. Dupuis, Phys. Rev. A **71**, 033629 (2005).
[31] M. Jreissaty, J. Carrasquilla, F. A. Wolf, and M. Rigol, Phys. Rev. A **84**, 043610 (2011).
[32] M. Aidelsburger, M. Atala, S. Nascimbene, S. Trotzky, Y.-A. Chen, and I. Bloch, Phys. Rev. Lett. **107**, 255301 (2011).
[33] J. Struck, C. Olschlager, R. Le Targat, P. Soltan-Panahi, A. Eckardt, M. Lewenstein, P. Windpassinger, and K. Sengstock, Science **333**, 996 (2011).
[34] C. Weitenberg, P. Schauss, T. Fukuhara, M. Cheneau, M. Endres, I. Bloch, and S. Kuhr, Phys. Rev. Lett. **106**, 215301 (2011).

[35] T.-L. Ho and S. Zhang, Phys. Rev. Lett. **107**, 150403 (2011).
[36] X. Zhou, Y. Li, Z. Cai, and C. Wu, J. Phys. B: At. Mol. Opt. Phys. **46**, 134001 (2013); C. Wu, I. M. Shem, and X.-F. Zhou, Chin. Phys. Lett. **28**, 097102 (2011).
[37] K. V. Krutitsky and P. Navez, Phys. Rev. A **84**, 033602 (2011).
[38] A. J. Leggett, Rev. Mod. Phys. **47**, 331 (1975).
[39] S. B. Chung, S. Raghu, A. Kapitulnik, and S. A. Kivelson, Phys. Rev. B **86**, 064525 (2012).